Extension of scaled particle theory to inhomogeneous hard particle fluids. I. Cavity growth at a hard wall

Daniel W. Siderius and David S. Corti*
School of Chemical Engineering, Purdue University, 480 Stadium Mall Drive, West Lafayette, Indiana 47907-2100, USA
(Received 23 November 2004; published 25 March 2005)

The methods of traditional scaled particle theory (SPT) are used to develop an extended scaled particle theory that is now applicable to hard particle fluids confined by hard walls. The new theory, labeled inhomogeneous SPT (I-SPT), introduces the function $\overline{G}$ that describes the average value of the anisotropic density of hard particle centers contacting a cavity placed at or behind a hard wall. We present an exact relation describing $\overline{G}$ for certain cavity sizes and, similar to the original SPT, an accurate interpolation scheme for larger cavity radii. Given $\overline{G}$, the reversible work of inserting a cavity centered at or behind the hard wall can be estimated. The work predictions at low to moderate packing fractions are extremely accurate, though small deviations from simulation results become apparent at packing fractions close to the bulk hard sphere freezing transition. I-SPT also reveals the importance of the line tension in determining the free energy of cavity formation for cavities intersecting a hard wall, a term which has been previously neglected. Furthermore, this paper provides the initial groundwork needed to develop a more complete SPT-based theory that can accurately predict the depletion force between a hard particle and a hard structureless wall.

DOI: 10.1103/PhysRevE.71.036141 PACS number(s): 05.70.Ce, 05.20.−y, 61.20.−p, 82.70.Dd

I. INTRODUCTION

Scaled particle theory (SPT), introduced in 1959 [1], is a remarkably simple theory that has, over the years, generated useful insights into the behavior of hard particle fluids as well as soft fluids [2–8]. Some of the ideas of SPT are also particularly useful for the analysis of those colloidal dispersions that can be closely approximated by hard core potentials [9], though SPT has not been extensively applied to these systems. Since these dispersions exhibit behavior similar to hard particle fluids, an additional class of forces, known as depletion forces, arise due to excluded volume effects [10]. Consequently, these depletion forces are essentially entropic in origin and are important in governing fluid-fluid phase transitions, particle drift, and fluid structure [9,11–14]. Given the nature of these entropic effects, SPT appears to provide a reasonable starting point for producing accurate expressions of depletion forces in hard sphere colloids.

Recently, Corti and Reiss [7] used SPT-based expressions to describe the depletion force between a colloidal particle and a hard, structureless wall. The reliance upon the equivalence of cavities and hard particles yielded a relatively straightforward procedure for calculating the depletion force. In their approach, the work of cavity insertion was separated into two components, a surface area and a pressure-volume contribution, with SPT providing both of the needed pressure and surface (or boundary) tension expressions. The resulting predictions were qualitatively good, though problems arose both for small particle sizes and at high densities since the uniform fluid assumptions on which SPT is based are not correct for a fluid confined by hard walls. In addition, quantitative errors were attributed to the neglecting of the line tension that develops along the three-phase interface (where the cavity, wall, and fluid meet).

Nevertheless, SPT, with its reliance upon physical and geometric arguments, still remains an attractive approach to the study of depletion forces in hard sphere colloids. The main limitation with SPT, at least with respect to its ability to describe depletion effects, is that it is a theory originally developed to describe bulk uniform fluids. The effects of any nonuniformities that appear near a wall are not accounted for by SPT in its current form. Hence, the various physical and geometric ideas of SPT need to be modified to describe nonuniform fluids, thereby extending the range of applicability of SPT and, hopefully, the accuracy of its depletion force predictions. Our interest in this extension of SPT does not, however, lie entirely with the estimation of depletion forces. Applying the various exact conditions and methods of SPT to nonuniform fluids may also serve to generate new insights into the behavior of confined fluids, just as traditional SPT was able to do for uniform fluids.

Given the prior success of SPT, we are, therefore, interested in developing a so-called *inhomogeneous* SPT, where the nonuniform fluid density that develops near the hard wall is explicitly taken into account. This new inhomogeneous SPT utilizes many arguments similar to the traditional (bulk, uniform) SPT. For example, statistical geometry is again used to generate several exact conditions that ensure thermodynamic consistency. In particular, we develop an inhomogeneous SPT (I-SPT) directly applicable to the insertion of cavities that are centered at or behind a hard wall exposed to a three-dimensional hard sphere fluid. This system provides both a convenient starting point to test the extension of SPT to nonuniform fluids and the initial steps needed to develop more fully a SPT-based approach that can accurately predict the depletion force between a particle and a wall. A forthcoming paper will both use and extend the ideas presented

*Electronic address: dscorti@ecn.purdue.edu

here to describe more relevant cavity configurations (such as those centered in front of the wall).

In this work, we introduce the central function of I-SPT, $\overline{G}$, which is related to the average density of particle centers in contact with the surface of the cavity. This I-SPT function allows one to calculate the reversible work of cavity insertion and reveals some new information about the fluid structure surrounding cavities placed within confined hard particle fluids. In our companion paper [15], we discuss in more detail the behavior of the fluid structure that develops around a cavity intersecting a hard wall by analyzing an extension of a previously derived SPT integral equation [5,16,17]. Analysis of this integral equation yields important additional insights into the properties of the I-SPT function discussed here.

The paper is organized as follows. Section II reviews SPT as applied to bulk hard sphere fluids. Section III describes the relevant geometry of the hard particle fluid confined between hard structureless walls and presents the various equations of I-SPT for the three-dimensional hard sphere fluid. Section IV compares the predictions of I-SPT with the results of Monte Carlo simulations. Conclusions are presented in Sec. V.

II. REVIEW OF SCALED PARTICLE THEORY

Before presenting our extension of SPT to an inhomogeneous fluid of hard particles, it is worthwhile to review the concepts of SPT as applied to bulk hard particle fluids. SPT has been previously derived for one-, two-, and three-dimensional hard particle fluids [1,18] and hard particle mixtures [19,20]. We review the pure component three-dimensional case here to provide a foundation for the following sections.

SPT was originally developed by Reiss, Frisch, and Lebowitz [1] who identified several exact relations that govern the thermodynamic properties of uniform hard particle fluids. Some of these relations describe the free energy cost of inserting additional hard particle solutes of any size to the system. Specifically, the excess free energy cost was equated to the reversible work, $W(\lambda)$, of inserting at a given location an equivalent cavity into the system. The cavity of radius of at least λ, sometimes referred to as a λ-cule, is a spherical region devoid of hard particle centers. The cavity radius λ is related to the equivalent solute particle diameter σ_s and the solvent particle diameter σ by

$$\lambda = \frac{\sigma_s + \sigma}{2}. \tag{1}$$

The relationship between λ, σ_s, and σ is also illustrated in Fig. 1.

We begin by introducing the central function of SPT, $G(\lambda)$, in which $\rho G(\lambda)$ is defined as the local density of hard sphere centers in contact with the cavity surface and ρ is the bulk fluid density (see Fig. 1). $G(\lambda)$ is connected to the reversible work of inserting a cavity of radius λ through the normal definition of thermodynamic work [1]

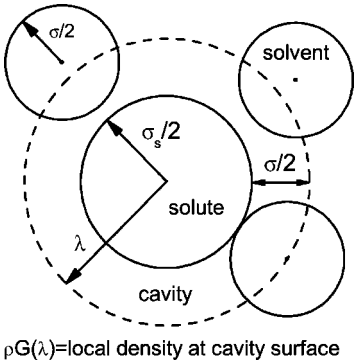

FIG. 1. Diagram illustrating the relationship between a cavity of radius of at least λ, the corresponding solute diameter σ_s, and solvent diameter σ. The center of each solvent particle may not penetrate the dashed line representing the cavity. The local density of hard sphere centers at the cavity surface is defined as $\rho G(\lambda)$ [1].

$$W(\lambda) = 4\pi\rho kT \int_0^\lambda G(r) r^2 dr. \tag{2}$$

This relation is obtained by integrating the kinetic pressure on the cavity surface, $\rho G(\lambda) kT$, over the volume of the cavity.

$G(\lambda)$ is also related to the probability of observing a spherical cavity of radius of at least λ within the fluid, denoted by $P_0(\lambda)$. From the definition of $G(\lambda)$, the probability of finding a particle center in a small spherical shell of width $d\lambda$ is equal to $4\pi\lambda^2\rho G(\lambda) d\lambda$, so that the probability of the same shell being empty is $1-4\pi\lambda^2\rho G(\lambda) d\lambda$. Now, the probability of finding a cavity of radius of at least $\lambda + d\lambda$, or $P_0(\lambda + d\lambda)$, is simply the probability of finding a cavity of radius λ multiplied by the probability of finding an empty spherical shell of width $d\lambda$, or

$$P_0(\lambda + d\lambda) = P_0(\lambda)[1 - 4\pi\lambda^2\rho G(\lambda) d\lambda]. \tag{3}$$

By expanding the left side of the above equation, rearranging, and taking the limit as $d\lambda \to 0$, one finds that [1]

$$G(\lambda) = \frac{-1}{4\pi\rho\lambda^2} \frac{\partial \ln P_0(\lambda)}{\partial \lambda}. \tag{4}$$

This equation could also have been derived using fluctuation theory, where $W(\lambda) = -kT \ln P_0(\lambda)$ [21].

Unfortunately, $P_0(\lambda)$ is not known in general, since it depends upon high-order correlation functions. Yet, the geometry of hard particle fluids provides an exact form for certain cavity radii [1]. For $\lambda \leqslant \sigma/2$, where cavities may contain at most one particle center, $P_0(\lambda)$ is given by $1-\rho v(\lambda)$, in which $v(\lambda) = 4\pi\lambda^3/3$ is the cavity volume. Applying this condition to Eq. (4) yields [1]

$$G(\lambda) = \frac{1}{1 - \frac{4}{3}\pi\rho\lambda^3} \quad \lambda \leqslant \frac{\sigma}{2}. \tag{5}$$

As may be expected, $G(0) = 1$ since the local density about a cavity of zero radius should be no different from the bulk, uniform density.

By examining the geometry of spherical cavities able to contain more than one particle, it was shown that both $G(\lambda)$ and $\partial G/\partial\lambda$ are continuous at $\lambda=\sigma/2$, but $\partial^2 G/\partial\lambda^2$ is discontinuous at $\lambda=\sigma/2$ [1]. Additional discontinuities occur in higher-order derivatives at larger λ [1]. $G(\lambda)$ is therefore nonanalytic for $\lambda>\sigma/2$, but can be approximated by a smooth function of λ. Despite being nonanalytic beyond $\sigma/2$, two other exact conditions on $G(\lambda)$ can still be generated. For $\lambda=\sigma$, in which the cavity is equivalent to another solvent particle via Eq. (1), $G(\sigma)$ is equal to the pair correlation function at contact, $g(\sigma^+)$. For $\lambda\to\infty$, the kinetic pressure on the cavity surface must approach the bulk fluid pressure because the surface curvature is approaching zero, i.e., $\lim_{\lambda\to\infty}\rho G(\lambda)kT=p$. In order to utilize these exact matching conditions and estimate $G(\lambda)$ beyond $\sigma/2$, an approximate form of $G(\lambda)$ must be proposed. Using surface thermodynamic arguments for the work of formation of a macroscopic cavity, one can represent the work of cavity insertion as [1]

$$W(\lambda)=\frac{4}{3}\pi\lambda^3 p+4\pi\lambda^2\gamma_\infty\left(1-\frac{2\delta}{\lambda}\right)+\cdots, \tag{6}$$

where the first term is a pressure-volume work contribution and the second is a surface work contribution. In the second term, γ_∞ is the surface tension (or more properly the *boundary* tension) of a cavity of zero curvature (identical to a planar surface) and δ is the "Tolman length" accounting for the dependence of surface tension on curvature. In Eq. (6), p, γ_∞, and δ are functions of the uniform fluid density and proportional to kT [1]. When this expression is compared to Eq. (2), the following form of $G(\lambda)$ is suggested [1]

$$G(\lambda)=\alpha_0(\rho)+\frac{\alpha_1(\rho)}{\lambda/\sigma}+\frac{\alpha_2(\rho)}{(\lambda/\sigma)^2}\quad\lambda>\frac{\sigma}{2}. \tag{7}$$

Each term in the above series is related to a thermodynamic work contribution from Eq. (6).

To solve for each $\alpha_i(\rho)$, three conditions are needed. The chosen conditions are the continuity of $G(\lambda)$ and $\partial G/\partial\lambda$ at $\sigma/2$ and the connection between $G(\infty)$ and $G(\sigma)$ via the virial equation of state (EOS) for hard spheres [1]

$$\frac{p}{\rho kT}=G(\infty)=1+\frac{2}{3}\pi\sigma^3\rho G(\sigma), \tag{8}$$

where $G(\sigma)$ has been substituted for $g(\sigma^+)$ and we reiterate that $G(\infty)=p/\rho kT$. After solving for each $\alpha_i(\rho)$, Eq. (7) can be combined with Eq. (5) and integrated via Eq. (2) to obtain the work of inserting a cavity of any size. In addition, solving for $G(\infty)$ in Eq. (7) yields the following EOS:

$$\frac{p}{\rho kT}=\frac{1+\eta+\eta^2}{(1-\eta)^3}, \tag{9}$$

where $\eta=\pi\rho\sigma^3/6$ is the dimensionless packing fraction. Curiously, this EOS is identical to the later derived Percus-Yevick compressibility EOS [22], and is the name by which Eq. (9) is most widely known.

It should be noted that five exact conditions on $G(\lambda)$ were originally derived, though only the three mentioned previously were applied to solve for the coefficients in Eq. (7) [1]. (All five were later used by Mandell and Reiss [19].) Continuing work [23] has generated two additional conditions, producing a more accurate EOS. If more than three conditions on $G(\lambda)$ are applied, thereby requiring more terms in the asymptotic representation of $G(\lambda)$, $\alpha_3(\rho)$ must be set to zero to suppress the appearance of logarithmic terms in $W(\lambda)$ that would appear upon integration of $G(\lambda)$ [3].

III. THEORETICAL DEVELOPMENT OF INHOMOGENEOUS SPT: CAVITIES INTERSECTING A HARD WALL

Our particular extension of bulk SPT to inhomogeneous fluids focuses on a pure component hard sphere fluid confined between hard structureless walls in both the positive and negative z directions with no confinements in the other Cartesian directions. The system is also chosen to be in the thermodynamic limit in which the distance between the two hard walls, and other directions as well, greatly exceeds the diameter of an individual particle. Hence, the identical nonuniformities that develop near each wall do not influence one another, so we are free to focus our attention on either the right or left wall. For each hard wall, the hard core of a particle may not penetrate the wall, meaning that the distance of closest approach of a particle center to the wall is $\sigma/2$ [see Fig. 2(a)]. The plane parallel to and measured a distance of $\sigma/2$ from the hard wall is therefore chosen, for convenience, to be the origin of the z axis, i.e., $z=0$. For $z<0$, the density of particle centers is uniformly zero. Thus, with respect to particle centers, the $z=0$ plane is an effective hard wall. For $z\geqslant 0$, the density of particle centers is given by $\rho(z)$, a function that begins at its contact value of $\rho(0)=p/kT$ and eventually dampens to the bulk density ρ. A typical plot of $\rho(z)$ obtained by Monte Carlo (MC) simulation (see Sec. IV A) is shown in Fig. 2(b).

For the systems considered in this paper, and in contrast to SPT as it has been applied to bulk uniform fluids, we focus on cavities whose surfaces intersect the $z=0$ plane. In particular, we restrict our attention to those cavities centered at $z\leqslant 0$. (Cavities centered at $z>0$ are handled separately in a forthcoming publication.) The portion of the cavity that extends beyond the $z=0$ plane is therefore hemispherical for $h=0$ or a spherical cap for $h<0$, where h denotes the z coordinate of the cavity center. Since the local density of particle centers surrounding a cavity that intersects the $z=0$ plane is not isotropic, the extension of SPT to inhomogeneous systems is facilitated by the introduction of curvilinear coordinates, shown in Fig. 3. The cavity radius λ originates from the geometric center of the cavity and the angle θ is measured from a line perpendicular to $z=0$ passing through the cavity center. The angle ϕ describes the rotation around this line. The system is symmetric about ϕ, though, because the x and y directions are indistinguishable due to a lack of confinement in these directions.

A. I-SPT for $h\leqslant 0$

I-SPT, or SPT of inhomogeneous hard sphere systems, begins with the equations of bulk SPT, though these relations

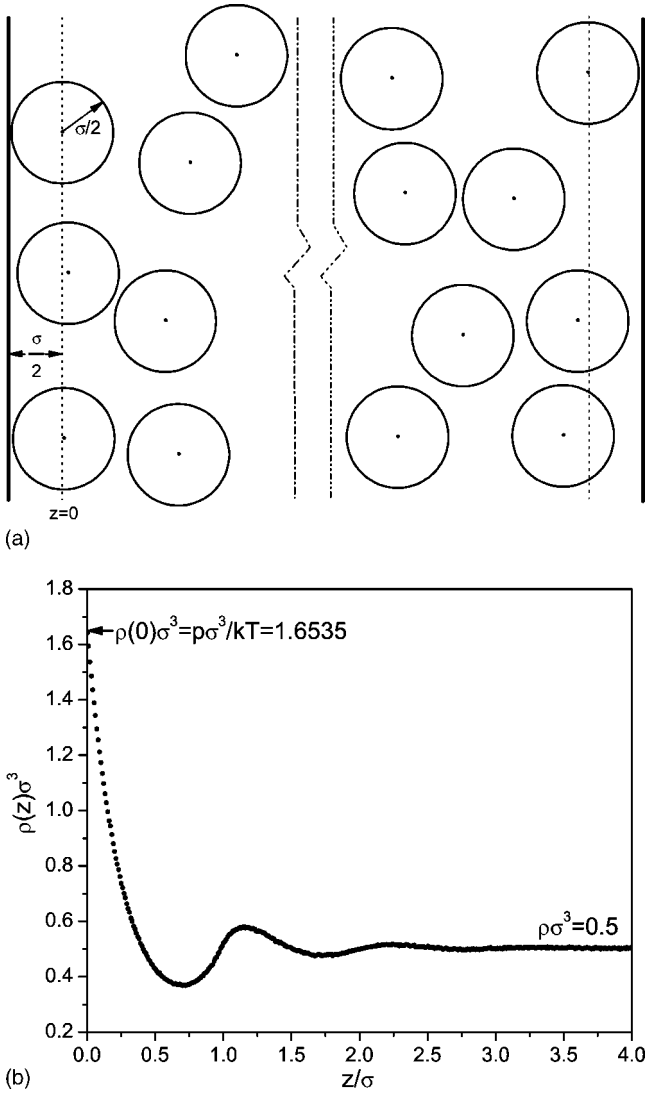

FIG. 2. (a) Two-dimensional representation of a hard sphere fluid confined between hard impenetrable walls at the z limits. The z axis orginates at a distance of $\sigma/2$ from the actual hard wall (where σ is the hard sphere diameter) and is perpendicular to the hard wall. (b) Inhomogeneous density profile $\rho(z)$ of hard spheres at a distance z from the hard wall for a bulk density $\rho\sigma^3=0.5$. $\rho(z)$ begins at its contact value of $\rho(0)=p/kT$ and decreases, while oscillating, to the bulk density ρ.

must be modified to account for both the intersection of a cavity with the hard wall and the resulting nonuniform density about the cavity. The pressure normal to the cavity surface remains solely kinetic and is still proportional to the local density of hard sphere centers contacting the cavity surface, but it must be recognized that this local density is a function of the far away bulk density ρ, the cavity radius λ, and now the center coordinate h and the angle θ. The θ-dependence arises from the anisotropic environment around the cavity induced by the hard wall.

Similar to bulk SPT, the inhomogeneous SPT function, $G(\lambda,\theta,h)$, is introduced, where $\rho G(\lambda,\theta,h)$ is defined as the local density of hard sphere centers at the angle θ that are in contact with the surface of a cavity of radius λ centered at

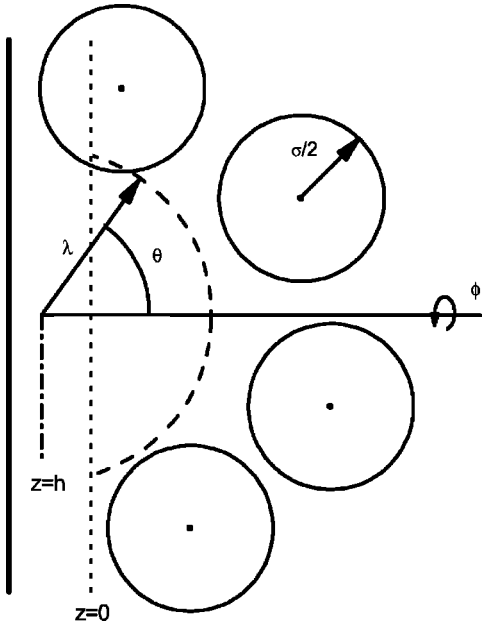

FIG. 3. Definition of the coordinate system used to analyze cavities centered at $z=h\leqslant 0$. λ is the radius of the cavity and θ is the angle measured from a line perpendicular to the $z=0$ plane. The local density of particle centers about the cavity is symmetric in ϕ. Only that portion of the cavity extending beyond $z=0$ is shown.

$z=h$. As before, $G(\lambda,\theta,h)$ is connected to the reversible work of inserting a cavity of radius λ at $z=h$ (so that the cavity intersects the hard wall) through

$$W(\lambda,h)=2\pi\int_{-h}^{\lambda}r^2dr\int_{0}^{\cos^{-1}(-h/r)}\rho G(r,\theta,h)kT\sin\theta\,d\theta, \tag{10}$$

where $\rho G(\lambda,\theta,h)kT$ has been substituted for the pressure normal to the cavity surface and is integrated over the appropriate r and θ-domains for fixed h. The lower bound on the r integral is $-h$, since for $\lambda<-h$ the cavity has not yet penetrated the fluid (so that $W(-h,h)=0$). The upper bound for θ follows from the point of intersection of the cavity and the $z=0$ plane, where $\cos\theta=-h/r$. The appearance of 2π follows from the integration over ϕ.

In order to relate $G(\lambda,\theta,h)$ to $P_0(\lambda,h)$, the probability of observing a cavity of radius of at least λ centered at $z=h$, we define the inhomogeneous analogue of Eq. (3). Given that the probability of observing a cavity of radius of at least $\lambda+d\lambda$, or $P_0(\lambda+d\lambda,h)$, is equal to the probability of finding a cavity of radius λ centered at $z=h$ multiplied by the probability of a concentric empty shell of width $d\lambda$, we find that

$$P_0(\lambda+d\lambda,h)=P_0(\lambda,h)\left(1-2\pi\rho\lambda^2d\lambda\int_{0}^{\cos^{-1}(-h/\lambda)}G(\lambda,\theta,h)\sin\theta\,d\theta\right). \tag{11}$$

Note that $G(\lambda,\theta,h)$ must be integrated over the θ-domain to determine the probability of finding an empty shell. It is

useful at this point to define a new function $\overline{G}(\lambda,h)$ by averaging $G(\lambda,\theta,h)$ over the relevant θ domain, resulting in

$$\overline{G}(\lambda,h)=\frac{2\pi\int_0^{\cos^{-1}(-h/\lambda)}G(\lambda,\theta,h)\sin\theta\,d\theta}{2\pi\int_0^{\cos^{-1}(-h/\lambda)}\sin\theta\,d\theta}=\frac{\lambda^2}{\lambda^2+\lambda h}\int_0^{\cos^{-1}(-h/\lambda)}G(\lambda,\theta,h)\sin\theta\,d\theta. \quad (12)$$

This average also allows $P_0(\lambda+d\lambda,h)$ and $W(\lambda,h)$ to be expressed more compactly as

$$P_0(\lambda+d\lambda,h)=P_0(\lambda,h)[1-2\pi\rho\overline{G}(\lambda,h)(\lambda^2+\lambda h)d\lambda], \quad (13)$$

$$W(\lambda,h)=2\pi\rho kT\int_0^{\lambda}\overline{G}(r,h)r(r+h)dr. \quad (14)$$

As in Sec. II, we now expand the left side of Eq. (13), combine terms, and take the limit as $d\lambda\to 0$. The result is

$$\rho\overline{G}(\lambda,h)=\frac{-1}{2\pi(\lambda^2+\lambda h)}\frac{\partial\ln P_0(\lambda,h)}{\partial\lambda}. \quad (15)$$

The determination of an exact form for $\overline{G}(\lambda,h)$ now requires that we identify an exact expression for $P_0(\lambda,h)$.

Consider the circle of intersection that is generated when the spherical cavity intersects the $z=0$ plane (this circle also lies in the $z=0$ plane). If the diameter of this circle of intersection is less than or equal to σ, i.e., $\lambda\leqslant\sqrt{h^2+(\sigma/2)^2}$, then that portion of the cavity to the right of $z=0$ can contain at most one solvent particle. Now, the probability of finding a particle center in this region is $\int_{v(\lambda,h)}\rho(\mathbf{r})d\mathbf{r}$, where $\rho(\mathbf{r})$ is the local density of centers (when no cavity is present) at a position $\mathbf{r}$ centered at $z=h$. The integral is evaluated over the volume of the cavity that extends to the right of $z=0$, or $v(\lambda,h)$. Consequently, $P_0(\lambda,h)$ is given by $1-\int_{v(\lambda,h)}\rho(\mathbf{r})d\mathbf{r}$. Since the density, $\rho(\mathbf{r})$, is most naturally a function of z [see Fig. 2(b)], we instead integrate $\rho(z)$ over a body of revolution corresponding to the cavity. For the three-dimensional cavities we consider, the revolved function is a circle whose area is $\pi[\lambda^2-(z-h)^2]$. Therefore,

$$P_0(\lambda,h)=1-\pi\int_0^{\lambda+h}\rho(z)[\lambda^2-(z-h)^2]dz,\qquad \lambda\leqslant\sqrt{h^2+\left(\frac{\sigma}{2}\right)^2}. \quad (16)$$

Finally, entering the above into Eq. (15) leads to the following *exact* relation

$$\rho\overline{G}(\lambda,h)=\frac{\int_0^{\lambda+h}\rho(z)dz}{(\lambda+h)\left(1-\pi\int_0^{\lambda+h}\rho(z)[\lambda^2-(z-h)^2]dz\right)},\qquad \lambda\leqslant\sqrt{h^2+\left(\frac{\sigma}{2}\right)^2}. \quad (17)$$

This exact expression for $\overline{G}(\lambda,h)$ can be checked for thermodynamic consistency by examining its limit for small cavities. When $\lambda\to -h$ [or $v(\lambda,h)\to 0$], the pressure on the cavity surface should approach the pressure that is exerted on the $z=0$ plane when no cavity is present. In other words, $\rho\overline{G}(-h,h)kT=p$, the bulk pressure. With the aid of L'Hopital's rule, Eq. (17) indicates that

$$\overline{G}(-h,h)=\lim_{\lambda\to -h}\overline{G}(\lambda,h)=\frac{\rho(0)}{\rho}=\frac{p}{\rho kT}, \quad (18)$$

where $\rho(0)=p/kT$ is the contact value of the density profile $\rho(z)$.

Another interesting property of $\overline{G}(\lambda,h)$ is found by examining its first derivative with respect to λ for λ approaching $-h$. Differentiation followed by the application of L'Hopital's rule yields the following result for the slope of $\overline{G}(\lambda,h)$ at $\lambda=-h$:

$$\lim_{\lambda\to -h}\frac{\partial\overline{G}}{\partial\lambda}=\frac{1}{2\rho}\left.\frac{d\rho(\lambda+h)}{d\lambda}\right|_{\lambda=-h}=\frac{1}{2\rho}\left.\frac{d\rho(z)}{dz}\right|_{z=0}\leqslant 0, \quad (19)$$

where the second equality results from a change of variables, and we note that for hard sphere fluids the initial slope of the density profile at a hard wall is never positive [see Fig. 2(b)]. The initial negative slope implied by Eq. (19) provides an interesting constraint on the qualitative behavior of $\overline{G}(\lambda,h)$.

For example, consider the limiting behavior of $\overline{G}(\lambda,h)$ as $\lambda\to\infty$. As λ becomes very large, the surface of the cavity will begin to resemble a planar surface, or flat hard wall, so that $\overline{G}(\infty,h)$ should be equal to $p/\rho kT$ [just like $G(\infty)$ in bulk SPT]. There is, of course, a small wedge-shaped [24] region localized about the point of intersection of the cavity surface and the $z=0$ plane where the surrounding fluid will not behave as if next to a hard wall for any value of λ. In fact, the local density within this wedge exceeds the hard wall limit of $p/\rho kT$ (see our companion paper [15] for a more detailed discussion of the density profile surrounding a cavity that intersects the hard wall). The effects of this density enhancement do not, however, propagate much beyond the wedge region for large cavity radii. Hence, as $\lambda\to\infty$, the wedge region (whose surface area is becoming an ever smaller fraction of the total surface area of the cavity) yields a negligibly small affect on $\overline{G}(\lambda,h)$. Therefore, one can state with confidence that $\lim_{\lambda\to\infty}\overline{G}(\lambda,h)=p/\rho kT$, thereby providing another exact condition on $\overline{G}(\lambda,h)$. Whether $\overline{G}(\lambda,h)$ ap-

proaches this limit from values above or below $p/\rho kT$ is not specified. In the Appendix, we present a thermodynamic argument that strongly suggests that $\overline{G}(\lambda,h)$ approaches its infinite limit from values below $p/\rho kT$. Given this result and the accurate form of $\overline{G}(\lambda,h)$ proposed in the next section, it is also likely that $\overline{G}(\lambda,h)$ never exceeds $p/\rho kT$.

Now, if both conditions, $\overline{G}(-h,h)=p/\rho kT$ and $\overline{G}(\infty,h)=p/\rho kT$, are to be met along with the initially negative slope required by Eq. (19), we conclude that $\overline{G}(\lambda,h)$ must exhibit a minimum at some intermediate value of λ. This behavior is quite different from what is exhibited by the bulk $G(\lambda)$, which begins at unity and rises to the final value of $G(\infty)=p/\rho kT$, where $\partial G/\partial\lambda \geqslant 0$ for all λ. In particular, our results show that for $h=0$ (hemispherical cavity), the minimum in $\overline{G}(\lambda,h)$ always appears in the range of $0\leqslant\lambda\leqslant\sigma/2$ where $\overline{G}(\lambda,0)$ is known exactly from Eq. (17). [We have been unable to prove this formally via Eq. (17) since $\rho(z)$ is not known in general. Though, the use of $\rho(z)$ generated from molecular simulation always yields a minimum of $\overline{G}(\lambda,h)$ for $h=0$ within $0\leqslant\lambda\leqslant\sigma/2$, at least for densities up to $\rho\sigma^3=0.914$.] For a more thorough examination of the decrease of and minimum in $\overline{G}(\lambda,h)$ (specifically for $h=0$), the reader is referred to our accompanying paper [15].

The initial decrease in $\overline{G}(\lambda,h)$ also implies that the average density of spheres in contact with the cavity surface decreases as the cavity grows in size (and begins to extend beyond the $z=0$ plane). Given that a local density enhancement above p/kT appears at the point of intersection between the cavity surface and the $z=0$ plane [15], the initial decrease in $\overline{G}(\lambda,h)$ implies that the local density at the front of the cavity ($\theta\approx 0$) drops quite rapidly, yielding a net decrease in $\overline{G}(\lambda,h)$. Again, this anisotropic behavior is not observed in bulk SPT.

Using Eq. (17), along with an accurate density profile $\rho(z)$ enables one to generate $\overline{G}(\lambda,h)$ up to the exact limit of $\lambda=\sqrt{h^2+(\sigma/2)^2}$. Beyond this limit, the form of $\overline{G}(\lambda,h)$ is not known. Hence, as in bulk SPT, the description of $\overline{G}(\lambda,h)$ for larger cavities requires the introduction of a function that utilizes some amount of exact information, if known, about $\overline{G}(\lambda,h)$. For example, in the original SPT paper, both $G(\lambda)$ and $\partial G/\partial\lambda$ are shown to be continuous at the exact limit of $\lambda=\sigma/2$. Invoking similar arguments for our inhomogeneous system suggests that $\overline{G}(\lambda,h)$ and $\partial\overline{G}/\partial\lambda$ are also continuous at the exact limit of $\lambda=\sqrt{h^2+(\sigma/2)^2}$. **(**Likewise, $\partial^2\overline{G}/\partial\lambda^2$ should also be discontinuous at $\sqrt{h^2+(\sigma/2)^2}$, though this condition appears to be of limited use. In addition, continuing work suggests that not only may $\partial^2\overline{G}/\partial\lambda^2$ be discontinuous, but that it likely diverges for $\lambda\rightarrow\sqrt{h^2+(\sigma/2)^2}$ from above. The determination of $\partial^2\overline{G}/\partial\lambda^2$ for values infinitesimally larger than $\sqrt{h^2+(\sigma/2)^2}$ appears to reduce to the two-dimensional problem of determining circular areas of overlap. $\partial^2\overline{G}/\partial\lambda^2$ should therefore diverge just as $\partial^2 G/\partial\lambda^2$ does for the unconfined two-dimensional hard disk fluid [18].**)** Consequently, $\overline{G}(\lambda,h)$ and $\partial\overline{G}/\partial\lambda$ at $\lambda=\sqrt{h^2+(\sigma/2)^2}$, known from Eq. (17), provide us with our first two exact matching conditions. A third exact condition follows from the behavior of $\overline{G}(\lambda,h)$ at $\lambda\rightarrow\infty$, where, as discussed earlier, we have that $\overline{G}(\infty,h)=p/\rho kT$. A further condition can also be generated, but the nature of this additional constraint and whether it is exact, is specific for $h=0$ and $h<0$. In other words, a fourth exact condition that is available for hemispherical cavities is not applicable to cavities shaped like spherical caps. For $h<0$, we introduce a fourth condition based on a semiempirical argument.

B. Interpolation for hemispherical cavity: $h=0$

Let us begin by considering the growth of a hemispherical cavity centered at $z=h=0$. For notational convenience, we drop the explicit reference to $h=0$ in $\overline{G}(\lambda,h)$ and relabel the I-SPT function simply as $\overline{G}(\lambda)$. From Eq. (17), the hemispherical I-SPT function for $\lambda\leqslant\sigma/2$ is given exactly by

$$\rho\overline{G}(\lambda)=\frac{\displaystyle\int_0^\lambda \rho(z)dz}{\lambda\left(1-\pi\displaystyle\int_0^\lambda \rho(z)(\lambda^2-z^2)dz\right)} \quad \lambda\leqslant\frac{\sigma}{2}. \tag{20}$$

In addition, the work of cavity formation is equal to

$$W(\lambda)=2\pi\rho kT\int_0^\lambda \overline{G}(r)r^2dr. \tag{21}$$

To interpolate $\overline{G}(\lambda)$ between its exact limit of $\lambda=\sigma/2$ and the limit of $\overline{G}(\lambda\rightarrow\infty)$, we invoke the macroscopic thermodynamic arguments used in bulk SPT and propose to represent $\overline{G}(\lambda)$ with the following four-term asymptotic series

$$\overline{G}(\lambda)=\beta_0(\rho)+\frac{\beta_1(\rho)}{(\lambda/\sigma)}+\frac{\beta_2(\rho)}{(\lambda/\sigma)^2}+\frac{\beta_4(\rho)}{(\lambda/\sigma)^4} \quad \lambda>\frac{\sigma}{2}. \tag{22}$$

The inclusion of a fourth term in Eq. (22) can be thought of as accounting for the "three-phase" line tension contribution to $W(\lambda)$ (where the hard sphere fluid, hard wall, and cavity comprise the three phases that meet at a circle lying in the $z=0$ plane). Note that $\beta_3(\rho)$ has been set to zero to suppress the appearance of logarithmic terms in $W(\lambda)$ [3].

Application of Eq. (22) requires the use of four matching conditions. As mentioned in the previous section, three conditions are the continuity of $\overline{G}(\lambda)$ and $\partial\overline{G}/\partial\lambda$ at $\lambda=\sigma/2$ [determined via Eq. (20)] and $\overline{G}(\infty)=p/\rho kT$. A fourth matching condition is available for $\lambda=\sigma$ (when the cavity is equivalent to another hard sphere) via the potential-distribution theory of Widom [25,26]. Given that the density of hard particle centers at some position z is proportional to the exponential of the work required to insert a hard particle at that z location, the ratio of the contact density, $\rho(0)$, of the fluid density profile to the bulk density ρ, is equal to

$$\frac{\rho(0)}{\rho} = \exp\left(-\frac{W(\sigma) - W_\infty(\sigma)}{kT}\right) = \frac{p}{\rho kT}, \tag{23}$$

where $W(\sigma)$ is the work of inserting another hard sphere or cavity of radius σ at $z=0$, and $W_\infty(\sigma)$ is the work of inserting the same particle or cavity in the bulk ($z\to\infty$) fluid. $W_\infty(\sigma)$ is numerically identical to the excess chemical potential (μ^{ex}) of the hard sphere fluid while $W(\sigma)$ can be calculated from $\overline{G}(\lambda)$ using equation (21).

Because this inhomogeneous theory does not connect $\overline{G}(\lambda)$ to the bulk radial distribution function at contact, the determination of each $\beta_i(\rho)$ in equation (22) does not produce an approximate EOS. This approach requires the use of an independent EOS to calculate $p/\rho kT$ and $W_\infty(\sigma)$ *a priori*. (p and $W_\infty(\sigma)$ could be calculated via simulation, but we use an independent EOS to preserve a link between I-SPT and bulk SPT.) The Percus-Yevick (PY) EOS derived by bulk SPT was used to generate the results for most densities in this paper. Our I-SPT method is, however, flexible enough to use another EOS, such as the Carnahan-Starling (CS) EOS [27], or even molecular simulation data.

With four matching conditions identified and an EOS having been chosen, each $\beta_i(\rho)$ can now be determined by simultaneous solution of the relevant equations. Note that the condition on $\overline{G}(\lambda)$ as $\lambda\to\infty$ requires that $\beta_0(\rho)=p/\rho kT$. After each $\beta_i(\rho)$ is determined, one can calculate the work of insertion for any sized hemispherical cavity through the use of equation (21).

C. Interpolation for spherical cap-shaped cavity: $h<0$

Like the hemispherical case, we again use an asymptotic function to represent $\overline{G}(\lambda,h)$ beyond the exact limit. We propose to represent $\overline{G}(\lambda,h)$ for $h<0$ with the following four-term asymptotic series:

$$\overline{G}(\lambda,h) = \beta_0(\rho,h) + \frac{\beta_1(\rho,h)}{(\lambda+h)/\sigma} + \frac{\beta_2(\rho,h)}{\lambda(\lambda+h)/\sigma^2} + \frac{\beta_4(\rho,h)}{\lambda^3(\lambda+h)/\sigma^4}, \quad \lambda > \sqrt{h^2+\left(\frac{\sigma}{2}\right)^2}, \tag{24}$$

where $\beta_i(\rho,h)$ are the matching coefficients. This series was chosen from a list of possible functions as the one which best matched simulation data, in addition to reducing to Eq. (22) for $h=0$. The three previously mentioned exact matching conditions of $\lim_{\lambda\to\infty}\overline{G}(\lambda,h)=p/\rho kT$ and the continuity of both $\overline{G}(\lambda,h)$ and $\partial\overline{G}(\lambda,h)/\partial\lambda$ at the exact limit still apply here. The other matching condition obtained from Widom's potential-distribution theory [25,26] is, however, not valid in this case because a cavity centered at $h<0$ is never equivalent to a solvent particle. Instead, we develop a fourth matching condition using a semiempirical argument: as λ becomes large relative to $|h|$, one may expect the cavity to behave like a hemispherical cavity, i.e., the distribution of hard sphere centers around the nonhemispherical cavity should be nearly identical to that surrounding a hemispherical cavity of equal radius. In other words, we expect the value of $\rho\overline{G}(\lambda,h)$ to be very near $\rho\overline{G}(\lambda)$ for $\lambda\gg -h$. Although reasonable, this condition was partly deduced by analyzing the behavior of $\overline{G}(\lambda,h)$ as obtained by simulation. Hence, our fourth, but not exact, matching condition is chosen to be $\overline{G}(\lambda_{\text{match}},h)=\overline{G}(\lambda_{\text{match}})$ for some sufficiently large value of λ_{match}. Clearly, the choice of λ_{match} will depend upon the value of h, and so a single value of λ_{match} cannot be used to describe all (ρ,h) combinations. As an example, we found for $-\sigma<h<0$ that numerical predictions agreed quite well with simulation results for $\lambda_{\text{match}}=4\sigma$. Larger values of λ_{match} did not provide additional accuracy.

IV. RESULTS

We present several tests of the accuracy of I-SPT, in which the predictions of $W(\lambda,h)$ obtained from I-SPT are compared to the results of molecular simulation. To accomplish this, I-SPT requires some expression, either analytical or numeric, for the density profile $\rho(z)$. Approximate expressions of $\rho(z)$ for hard sphere fluids have been developed using hypernetted chain and superposition approximations [28,29], but these approximations are not sufficiently accurate for extending SPT to inhomogeneous fluids at densities higher than about $\rho\sigma^3=0.4$. We, therefore, chose to use density profiles generated directly by Monte Carlo simulation. This is not a drawback, however, since highly accurate density profiles can be obtained via simulation with little computational effort. In addition, I-SPT, unlike bulk SPT, does not yield information on the properties and structure of the hard sphere fluid near a wall. For example, I-SPT requires that an independent EOS be introduced to calculate $\overline{G}(\infty,h)=p/\rho kT$. Likewise, $\rho(z)$ must be determined outside of I-SPT. Nevertheless, I-SPT is flexible enough such that future analytical approximations for $\rho(z)$, when they become as accurate as simulation profiles, can be directly incorporated into I-SPT.

A. Simulation method

The comparison with simulation results requires that both $\rho(z)$ and $W(\lambda,h)$ be determined computationally. We generated all relevant data by MC simulations in an isothermal-isobaric (constant N,p,T) ensemble with hard walls. All variables were scaled using characteristic values for hard particle systems. The number of particles used in the various simulations was adjusted to ensure that a uniform fluid phase with the appropriate bulk properties developed in the center of the simulation cell. Depending on the chosen density, the system size ranged from 500 to 3000 particles. Each simulation was run for a target density in the center of the simulation cell, with the imposed pressure being calculated from the PY EOS [1] to ensure consistency between the interior density ρ, the density profile $\rho(z)$, and the wall contact density $\rho(0)=p/kT$. Hard walls were imposed at the z limits of the simulation cell and periodic boundary conditions were applied in the x and y directions. The x and y dimensions of the simulation cell were large enough to prevent a particle or cavity "seeing" its mirror image. As a rule of thumb, these dimen-

sions were at least $4\lambda_{max}$, where λ_{max} was the largest cavity radius probed by the simulation. The simulations were allowed to equilibrate before recording results for a sufficient number of cycles, typically 3×10^4 to 10^5, each cycle including N particle translations and one volume adjustment. Volume moves were accomplished by adjusting only the length of the cell in the z direction of the simulation cell [30,31] and accepted according to standard NpT acceptance criteria [32], while translational moves were accomplished by randomly moving particles and looking for particle overlap. Simulation density profiles were generated by measuring the local density as a function of z and averaging each z bin over the length of the simulation. Results were collected over a production run of 10^6 to 5×10^6 cycles.

The reversible work of cavity insertion for different λ and h was calculated from the probability of observing cavities along the hard wall. To determine $W(\lambda,h)$ for large cavity sizes (generally $\lambda>1.5\sigma$), an umbrella sampling technique [32] was used in which windows of progressively larger radii were probed. Within each simulation window, a cavity was placed into on the system and grown or shrunk radially as an extra MC trial "move" each cycle. The cavity move was controlled according to a biasing potential, $\psi(\lambda)$. Good statistics are achieved when $\psi(\lambda)=-W(\lambda)$, so we used a polynomial regression of the previously collected cavity work profile to compute $\psi(\lambda)$ [33]. After each window, the most recent probability histogram was normalized according to the biasing potential and linked with the previously collected work data to obtain the updated cavity work profile. With this method, we were able to determine work profiles up to cavity radii around 3σ. Beyond this size and for moderate to high densities, the large system sizes required and the large number of windows needed, as a result of the ever-increasing steepness of $W(\lambda)$, made this simulation technique too computationally expensive.

B. Hemispherical cavity: $\bar{G}(\lambda)$ and $W(\lambda)$

Once the density profile $\rho(z)$ and bulk pressure p/kT are known, both $\bar{G}(\lambda)$ and $W(\lambda)$ for cavities centered at $z=0$ can be obtained using the equations shown in Sec. III B. Determining $\rho(z)$ directly from simulation allows us to calculate $\bar{G}(\lambda)$ "exactly" for $\lambda\leqslant\sigma/2$ using Eq. (20). $\bar{G}(\lambda)$, and thereby $W(\lambda)$, were calculated analytically for $\lambda>\sigma/2$ using the series approximation given by Eq. (22), where the four hemispherical matching conditions were invoked to solve for each $\beta_i(\rho)$.

Figure 4 displays the hemispherical I-SPT function $\bar{G}(\lambda)$ for the bulk densities $\rho\sigma^3=0.1$, 0.3, 0.5, and 0.6. Also included for comparison is the corresponding bulk SPT function $G(\lambda)$ at $\rho\sigma^3=0.3$. $\bar{G}(\lambda)$ begins at $p/\rho kT$ for $\lambda=0$ and, as expected from Eq. (19), has an initially negative slope. In the limit of $\lambda\to\infty$, $\bar{G}(\lambda)$ again approaches $p/\rho kT$. Note that $G(\infty)=p/\rho kT$ as well. In general, $\bar{G}(\lambda)$ approaches the infinite limit much faster than $G(\lambda)$, as seen by the comparison of these two functions presented in Fig. 4 for $\rho\sigma^3=0.3$. In fact, for the bulk densities shown, $\bar{G}(\lambda)$ reaches a value of at least 95% of its infinite limit within a cavity radius of only four particle diameters. The bulk $G(\lambda)$ requires a radius of approximately eight particle diameters to reach the same value.

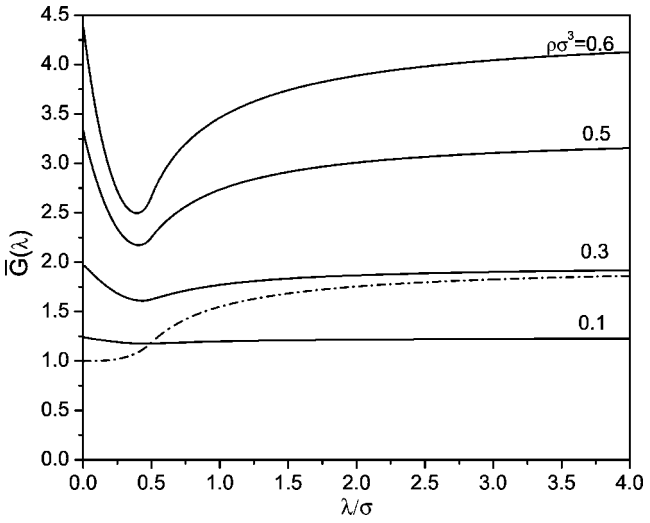

FIG. 4. Three-dimensional inhomogeneous SPT function $\bar{G}(\lambda)$ for the bulk densities $\rho\sigma^3=0.1$, 0.3, 0.5, and 0.6. For comparison, the dashed line denotes the bulk SPT function $G(\lambda)$ for $\rho\sigma^3=0.3$. For all densities, both $\bar{G}(0)$ and $\bar{G}(\infty)$ are equal to $p/\rho kT$. Note that the minimum in each $\bar{G}(\lambda)$ always occurs before $\lambda=\sigma/2$.

As argued previously, and as a consequence of Eq. (19), $\bar{G}(\lambda)$ exhibits a minimum at some intermediate radius. A more detailed inspection of Fig. 4 also reveals that this minimum always occurs before $\lambda=\sigma/2$. The minimum of $\bar{G}(\lambda)$ is not, however, located at the same value of z where the first minimum of the density profile $\rho(z)$ is found. [See Fig. 2(b); in general, the first local minimum of $\rho(z)$ may be located at a value of z either greater than or less than $\sigma/2$.] Nevertheless, there is a connection between these two minima. The radius λ at which the minimum in $\bar{G}(\lambda)$ occurs decreases with an increase in the bulk density ρ, just as the value of z at which the $\rho(z)$ reaches its first local minimum decreases with an increase in ρ. When $\rho(z)$ is integrated in Eq. (20), this behavior becomes part of $\bar{G}(\lambda)$ because the successive integration volumes appearing in Eq. (20) yield smaller and smaller contributions.

Ultimately, the minimum in $\bar{G}(\lambda)$ implies that the average density of particle centers at the cavity surface is less than the hard wall contact value of $\rho(0)=p/kT$. Equation (20) does not provide information on the local structure, or θ-dependence of the density profile around the cavity. We further investigate the minimum in $\bar{G}(\lambda)$ in our companion paper [15], analyzing the local structure that develops around the hemispherical cavity. Interestingly, we find that $\bar{G}(\lambda)$ initially decreases despite the appearance of a local density enhancement above p/kT at the point of intersection between the cavity and the $z=0$ plane.

The true test of I-SPT and the various relations describing $\bar{G}(\lambda)$ is to compare the I-SPT work predictions for $W(\lambda)$ with

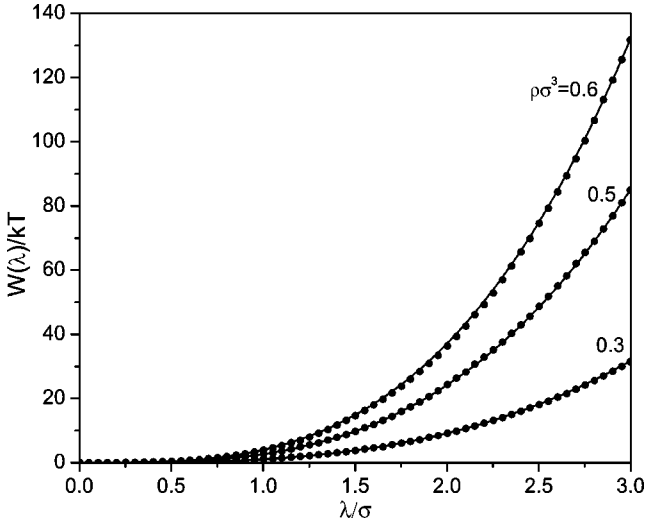

FIG. 5. Reversible work of insertion $W(\lambda)$ for hemispherical cavities of various radii λ centered at $z=0$ for $\rho\sigma^3=0.3$, 0.5, and 0.6. Solid lines represent the work predictions I-SPT while the closed circles represent MC simulation data.

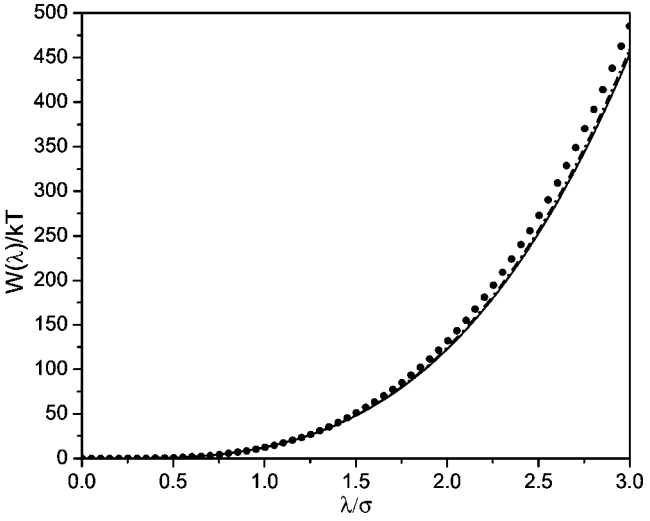

FIG. 6. Reversible work of cavity insertion $W(\lambda)$ for cavities of radius λ centered at $z=0$ for a reduced bulk presure $p\sigma^3/kT=10.308$. The closed circles represent the MC simulation data, the dashed line denotes I-SPT results based on the PY EOS, and the solid line represents I-SPT results using the Carnahan-Starling (CS) EOS. The corresponding interior density from the PY EOS is $\rho\sigma^3=0.9$, while that from the CS EOS is $\rho\sigma^3=0.914$. Both densities are near the bulk hard sphere freezing transition ($\rho_{\text{freezing}}\sigma^3=0.949$ [34–36]). At $\lambda=3\sigma$, the deviation between the CS-based predictions and simulation data is $\approx 31kT$ corresponding to a 6.4% underprediction. At the same point, the error in the PY-based predictions is $\approx 25kT$, corresponding to a 5.1% underprediction.

the results of MC simulation. Figure 5 shows for several bulk densities the values of $W(\lambda)$ obtained from $\bar{G}(\lambda)$, via Eq. (21), along with $W(\lambda)$ determined directly from simulation. Overall, the agreement between simulation and I-SPT is excellent, at least up to $\lambda=3\sigma$. In particular, works of cavity growth are predicted with high accuracy for values of $W(\lambda)$ in excess of $100kT$. For example, the error for $\rho\sigma^3=0.6$ at $\lambda=3\sigma$ is less than 0.2%. MC simulation becomes inefficient for radii greater than 3σ due to sampling difficulties. Inhomogeneous SPT should, however, continue to accurately predict $W(\lambda)$ beyond 3σ since, as seen in Fig. 4, $\bar{G}(\lambda)$ rapidly approaches its infinite limit beyond $\lambda=3\sigma$. For larger radii, the interfacial contributions to $W(\lambda)$ will become increasingly small compared to the leading order pressure-volume contribution.

I-SPT can be subjected to a more rigorous test by examining its predictions for a fluid pressure whose bulk density is near the hard sphere freezing transition ($\rho_{\text{freezing}}\sigma^3=0.949$ [34–36]). Figure 6 compares simulation data to theoretical predictions for a reduced pressure of $p\sigma^3/kT=10.308$ obtained using two different equations of state. At this high pressure, and since the EOS of the hard sphere fluid is not known exactly, the different EOSs yield different values of the bulk density ρ corresponding to the same pressure. For example, the SPT-derived PY EOS predicts that $\rho\sigma^3=0.9$, while the more accurate CS EOS predicts that $\rho\sigma^3=0.914$. (For reference, the bulk density in the simulation center was $\rho\sigma^3=0.911\pm0.005$ for this pressure.) Consequently, the predictions of I-SPT using the PY EOS should not accurately match data produced by MC simulation in an isothermal-isobaric ensemble in which the *pressure*, not the interior density, is fixed. Thus, a more accurate EOS may improve the predictions for $W(\lambda)$. Unfortunately, this is not observed in Fig. 6 where the predictions of I-SPT using the CS EOS yield an error comparable to I-SPT using the PY EOS when compared to simulation. The error for the CS-derived results is, in fact, slightly larger than that from the PY EOS. Using the CS EOS, good agreement between the I-SPT predictions and simulation data is found up to $\lambda=\sigma$ (as expected from using the matching condition at $\lambda=\sigma$), but I-SPT begins to underpredict $W(\lambda)$ for larger radii. This difference may be due to the MC simulation overpredicting the work of insertion or the error involved in using $W_\infty(\sigma)$ generated from the CS EOS [which may not match $W_\infty(\sigma)$ obtained directly from the simulation], or possibly the interpolation chosen for $\bar{G}(\lambda)$ not taking into account the discontinuity (and potential divergence) in $\partial^2\bar{G}/\partial\lambda^2$ at $\lambda=\sigma/2$. Yet, the I-SPT predictions are still reasonably accurate, as the error at $\lambda=3\sigma$ is only $\approx 31kT$ for $W(\lambda)$ around $480kT$, or approximately 6.4% error. At the same point, the error in the PY-based prediction is $\approx 25kT$, corresponding to a 5.1% underprediction.

C. Spherical cap

We now examine the accuracy of I-SPT results for cavities centered at $z<0$. As for $h=0$, $\bar{G}(\lambda,h)$ is calculated exactly by integrating $\rho(z)$ within a particular range of λ [see Eq. (17)]. Beyond this exact limit, an interpolation form, Eq. (24), is used to represent $\bar{G}(\lambda,h)$ in which the various coefficients are evaluated with the three exact conditions and a fourth semiempirical condition discussed in Sec. III C. $W(\lambda,h)$ is then calculated by integrating $\bar{G}(\lambda,h)$ via Eq. (14).

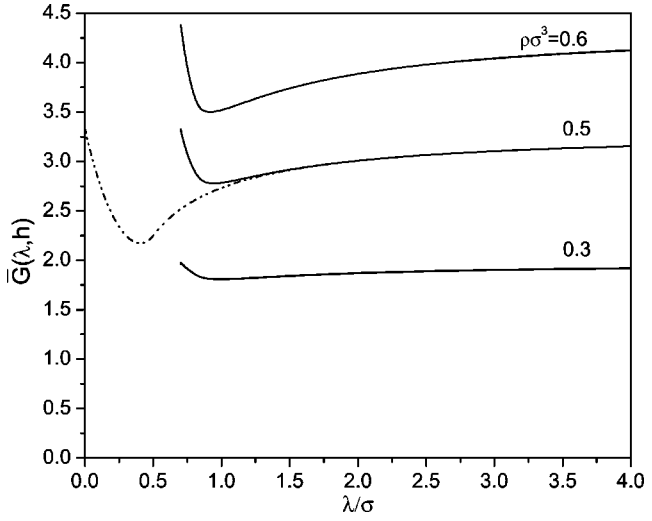

FIG. 7. The function $\bar{G}(\lambda,h)$ for cavities centered at $z=-0.7\sigma$ at bulk densities of $\rho\sigma^3=0.3$, 0.5, and 0.6. The dashed line shows the corresponding hemispherical $\bar{G}(\lambda)$ for $\rho\sigma^3=0.5$. The minima in $\bar{G}(\lambda,h)$ do not occur within the exact λ range of $0.7\sigma\leqslant\lambda\leqslant0.860\sigma$.

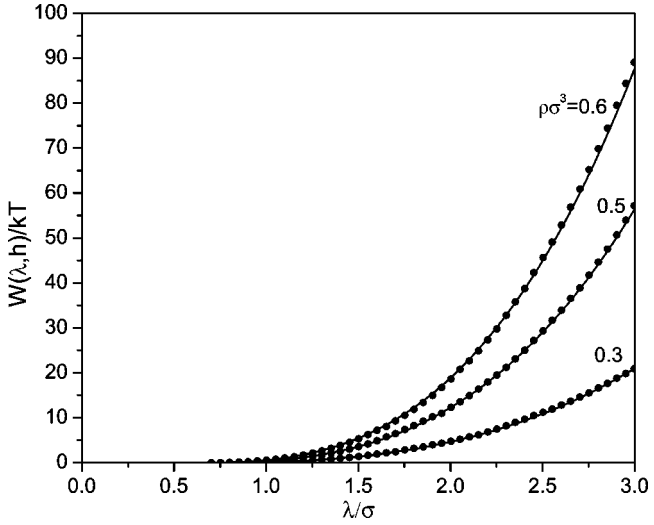

FIG. 8. Reversible work of cavity insertion $W(\lambda,h)$ for cavities centered at $z=-0.7\sigma$ at bulk densities $\rho\sigma^3=0.3$, 0.5, and 0.6. Solid lines represent I-SPT predictions and solid circles represent data generated by MC simulation.

Figure 7 shows $\bar{G}(\lambda,h)$ at various densities for cavities centered at $h=-0.7\sigma$. The exact range for this choice of h is $0.7\sigma\leqslant\lambda\leqslant0.860\sigma$. The radius used for the semiempirical condition, $\bar{G}(\lambda_{\text{match}})=\bar{G}(\lambda_{\text{match}},h)$, is $\lambda_{\text{match}}=4\sigma$. The hemispherical $\bar{G}(\lambda)$ at $\rho\sigma^3=0.5$ is shown for comparison. Qualitatively, $\bar{G}(\lambda,h)$ and the hemispherical $\bar{G}(\lambda)$ are the same. $\bar{G}(\lambda,h)$ satisfies the same limits of $p/\rho kT$ for $\lambda=-h$ and $\lambda\rightarrow\infty$ as $\bar{G}(\lambda)$, and also exhibits an initially negative slope. Quantitatively, however, the initial behavior of $\bar{G}(\lambda,h)$ differs greatly from $\bar{G}(\lambda)$. $\bar{G}(\lambda,h)$ decreases at a rate initially similar to $\bar{G}(\lambda)$, but the minimum of $\bar{G}(\lambda,h)$ occurs at a smaller relative distance, i.e., relative to the minimum value of λ. In addition, this minimum does not necessarily occur in the exact λ-range. For example, at $\rho\sigma^3=0.6$, the slope at the exact limit ($\lambda=0.860\sigma$) is $\bar{G}'(0.860\sigma,h)=-0.799/\sigma$, indicating that $\bar{G}(\lambda,h)$ is still decreasing. We must therefore rely on the interpolation function to predict the minimum. In this case, it is predicted to occur at $\lambda=0.92\sigma$ [corresponding to a relative distance of $0.92\sigma-0.7\sigma=0.2\sigma$; in comparison, at the same density, Fig. 4 reveals that the minimum of $\bar{G}(\lambda)$ occurs at a relative distance of 0.39σ]. After the minimum, $\bar{G}(\lambda,h)$ mimics the behavior of $\bar{G}(\lambda)$, rapidly becoming nearly identical in value to $\bar{G}(\lambda)$. The near equality of $\bar{G}(\lambda,h)$ and $\bar{G}(\lambda)$ at such small radii indicates that $\bar{G}(\lambda,h)$ is relatively insensitive to the value of λ_{match} used in the matching condition (as long as a sufficiently large value is selected). This behavior of $\bar{G}(\lambda,h)$ verifies our assumption that for cavities centered behind the $z=0$ plane ($h<0$), $\bar{G}(\lambda,h)$ eventually becomes identical to $\bar{G}(\lambda)$.

The near equivalence of $\bar{G}(\lambda,h)$ and $\bar{G}(\lambda)$ at such a small radius of $\lambda=2\sigma$ for $\rho\sigma^3=0.5$ is unexpected. For $\lambda=2\sigma$, the volume of the hemispherical cavity that extends to the right of $z=0$ is simply $16.76\sigma^3$. For $h=-0.7\sigma$, the cavity displaces only a volume of $8.32\sigma^3$, just 49.6% of the hemisphere. Thus, one might suspect that the local environment about each of these cavities will be quite different. Yet, the average of the local densities of sphere centers in contact with each cavity surface are identical.

Figure 8 shows the I-SPT predictions of the work of cavity insertion for the same densities chosen for Fig. 7. Again, there is good agreement between the simulation data and the theoretical predictions, at least up to $\lambda=3\sigma$. This agreement also indicates that the location of the minimum in $\bar{G}(\lambda,h)$ is predicted accurately by our chosen interpolation function [Eq. (24)]. Because $\bar{G}(\lambda,h)$ is close to the infinite limit at $\lambda=3\sigma$, the theory should continue to coincide with simulation results for larger λ. The theory does begin to underpredict $W(\lambda,h)$ near $\lambda=3\sigma$ at densities at and above $\rho\sigma^3=0.5$, which may be a consequence of the fewer exact number of matching conditions that can be generated for $h<0$. The underprediction is not large, however, as I-SPT yields an error of $\approx1.9\%$ at $\rho\sigma^3=0.6$ and $\lambda=3\sigma$.

V. CONCLUSION

An inhomogeneous scaled particle theory that provides theoretical methods for determining the reversible work of inserting a cavity near a hard structureless wall has been presented. The I-SPT predictions of the work of insertion are in good agreement with MC simulation results for the hard sphere fluid up to relatively large cavity sizes ($\lambda=3\sigma$) for all bulk densities below the fluid-solid transition. Thus, the exact equations of inhomogeneous SPT were confirmed and the proposed series interpolations of $\bar{G}(\lambda,h)$ were shown to be very accurate.

Perhaps the most striking consequence of I-SPT is that the average density of spheres in contact with cavity surface, or

$\overline{G}(\lambda,h)$, rapidly reaches a minimum value at small cavity radii before increasing to its infinite size limit of $p/\rho kT$. The minimum and the geometric reasons for its appearance are discussed in more detail in our companion paper [15]. Because the initial decrease of $\overline{G}(\lambda,h)$ implies that the average pressure on the cavity surface decreases, I-SPT confirms that the line tension developing at the three-phase interface (where the cavity, wall, and fluid meet) is important in governing the behavior of cavities placed at a hard wall. The decrease in $\overline{G}(\lambda,h)$ also suggests that the line tension is a negative quantity. The value of the line tension, of course, depends on the selection of the dividing surfaces. We have assumed that the dividing surface between the fluid and the cavity is convergent with the surface of the cavity and the dividing surface between the fluid and the wall is the $z=0$ plane. Selecting different locations could cause the line tension or boundary tension to become positive. The line tension, of course, becomes negligible for large cavities since $\overline{G}(\lambda,h)$ approaches the hard wall contact value of $p/\rho kT$. I-SPT may be used to determine numerical estimations of the line tension using the various relations of surface thermodynamics.

I-SPT can also be straightforwardly extended to the two-dimensional hard disk fluid confined by planar hard walls [37]. The equations are similar to those presented in this paper, but show minor changes due to the different system geometry. The behavior of the two-dimensional version of $\overline{G}(\lambda,h)$ is identical to that shown here, but $\partial\overline{G}/\partial\lambda$ at the exact limit is not used as a matching condition, like $G(\lambda)$ in bulk SPT for hard disks [18]. Work predictions from two-dimensional I-SPT also agree quite well with those from MC simulation, despite the discontinuity in $\partial\overline{G}/\partial\lambda$.

Finally, the ideas presented here provide the initial steps required for the development of an improved SPT-based method of calculating the depletion potentials and forces for a confined fluid. The work predictions for $\lambda\leqslant\sigma$ could be used to determine part of the depletion potential of a solute whose diameter is less than the hard particle diameter of σ. Our theory does not yet allow us to generate depletion potentials for $z>0$ or for solute diameters greater than σ. To calculate depletion potentials for $z>0$, an alternative approach must be developed in which a cavity is "pushed" into the fluid. Calculating the force in the z direction that opposes this "pushing" allows one to determine the work required to "push" the cavity into the fluid. Relations similar to $\overline{G}(\lambda,h)$ are needed to predict this force, i.e., a function $\overline{F}(\lambda,h)$ describing the net normal force (in the z direction) on the cavity surface centered at $z=h$ can be related to various statistical geometric quantities. I-SPT, as validated by the presented results, can be used to generate a crucial matching condition for this new function $\overline{F}(\lambda,h)$. The extension of I-SPT to describe $\overline{F}(\lambda,h)$ is the subject of a forthcoming paper.

ACKNOWLEDGMENTS

This material is based upon work supported by the National Science Foundation under Grant No. 0133780.

APPENDIX: SLOPE AND CURVATURE OF $\overline{G}(\lambda)$ AS $\lambda\to\infty$

As discussed in Sec. III, the asymptotic value of $\overline{G}(\lambda)$ is $p/\rho kT$. Whether $\overline{G}(\lambda)$ approaches this limit from above or below was not specified from its defining equations. Here, we present a thermodynamic argument that strongly suggests that $\overline{G}(\lambda)$ always approaches its asymptotic value from below.

From Eq. (21), the slope of $\overline{G}(\lambda)$ is given by

$$\frac{\partial\overline{G}}{\partial\lambda}=\frac{1}{2\pi\rho kT}\frac{\partial}{\partial\lambda}\left(\frac{1}{\lambda^2}\frac{\partial W}{\partial\lambda}\right). \tag{A1}$$

Since the work of formation, $W(\lambda)$, of a cavity intersecting the $z=0$ plane can also be thought of as arising from the sum of pressure-volume, surface area, and line tension contributions, one can write the following expression:

$$dW=pdV+d(\gamma_r A)+\gamma_\infty dA_{\text{wall}}+d(\tau_r L). \tag{A2}$$

In the above, τ_r is the line tension of the three-phase (cavity-fluid-wall) interface (based on a suitably chosen dividing surface), L is the length of this linear interface, A_{wall} is the area of the wall exposed to the fluid, γ_r is the boundary tension of a curved surface located a radius r from the cavity center and the remaining terms are as defined in Sec. II. For the hemispherical cavity centered at $z=0$, Eq. (A2) is transformed to

$$dW=p2\pi\lambda^2 d\lambda+d(\gamma_r 2\pi\lambda^2)-\gamma_\infty 2\pi\lambda d\lambda+d(\tau_r 2\pi\lambda), \tag{A3}$$

where the cavity-fluid dividing surface is chosen to be the same as the cavity surface ($r=\lambda$) and the three-phase interface is chosen to lie within the $z=0$ plane. After some straightforward algebra, one has

$$\frac{\partial}{\partial\lambda}\left(\frac{1}{\lambda^2}\frac{\partial W}{\partial\lambda}\right)=2\pi\frac{\partial^2\gamma_r}{\partial\lambda^2}-\frac{4\pi}{\lambda^2}\gamma_r+\frac{4\pi}{\lambda}\frac{\partial\gamma_r}{\partial\lambda}+\frac{2\pi}{\lambda^2}\gamma_\infty+\frac{2\pi}{\lambda}\frac{\partial^2\tau_r}{\partial\lambda^2}-\frac{4\pi}{\lambda^3}\tau_r. \tag{A4}$$

As the cavity becomes large, both the boundary tension γ_r and line tension τ_r may be approximated by the asymptotic functions [1]

$$\gamma_r=\gamma_\infty\left(1-\frac{2\delta}{\lambda}\right) \tag{A5}$$

and

$$\tau_r=\tau_\infty\left(1-\frac{\delta_t}{\lambda}\right). \tag{A6}$$

Entering these approximations into Eq. (A4) yields the following expression:

$$\frac{\partial}{\partial\lambda}\left(\frac{1}{\lambda^2}\frac{\partial W}{\partial\lambda}\right)=-\frac{2\pi}{\lambda^2}\gamma_\infty+\frac{8\pi\delta}{\lambda^3}\gamma_\infty-\frac{4\pi}{\lambda^3}\tau_\infty. \tag{A7}$$

Thus, the slope of $\overline{G}(\lambda)$, to the leading order, is

$$\frac{\partial \overline{G}}{\partial \lambda} = \frac{-1}{\rho kT}\frac{\gamma_\infty}{\lambda^2} + O(\lambda^{-3}), \tag{A8}$$

which is always positive because $\gamma_\infty \leq 0$. By taking an additional derivative of Eq. (A7), the second derivative of $\overline{G}(\lambda)$, to the leading order, is

$$\frac{\partial^2 \overline{G}}{\partial \lambda^2} = \frac{2}{\rho kT}\frac{\gamma_\infty}{\lambda^3} + O(\lambda^{-4}), \tag{A9}$$

which is always negative, indicating that $\overline{G}(\lambda)$ is concave down. Because $\overline{G}(\lambda)$ has both a positive slope and negative curvature as $\lambda \to \infty$, it will approach its asymptotic limit from values less than $p/\rho kT$. The above argument does not exclude the appearance above $p/\rho kT$ of a maximum in $\overline{G}(\lambda)$ at some cavity radius between $\lambda = \sigma/2$ and $\lambda = \infty$. Such a maximum, however, would require the structure of $\overline{G}(\lambda)$ to be much more complex than is currently thought. Simulation results, along with the overall accuracy of the I-SPT formalism, do not indicate that a maximum occurs above $p/\rho kT$ and are coincident with the conclusion that $\overline{G}(\lambda)$ always remains below its asymptotic limit.

[1] H. Reiss, H. L. Frisch, and J. L. Lebowitz, J. Chem. Phys. **31**, 369 (1959).
[2] H. Reiss, H. L. Frisch, E. Helfand, and J. L. Lebowitz, J. Chem. Phys. **32**, 119 (1960).
[3] D. M. Tully-Smith and H. Reiss, J. Chem. Phys. **53**, 4015 (1970).
[4] H. Reiss and D. M. Tully-Smith, J. Chem. Phys. **55**, 1674 (1971).
[5] H. Reiss and R. V. Casberg, J. Chem. Phys. **61**, 1107 (1974).
[6] A. Ben-Naim and R. Tenne, J. Chem. Phys. **67**, 627 (1977).
[7] D. S. Corti and H. Reiss, Mol. Phys. **95**, 269 (1998).
[8] S. M. Oversteegen and H. N. W. Lekkerkerker, J. Chem. Phys. **120**, 2470 (2004).
[9] A. D. Dinsmore, A. G. Yodh, and D. J. Pine, Phys. Rev. E **52**, 4045 (1995).
[10] S. Asakura and F. Oosawa, J. Chem. Phys. **22**, 1255 (1954).
[11] D. Frenkel, J. Phys.: Condens. Matter **6**, A71 (1994).
[12] X. Chu, A. D. Nikolov, and D. T. Wasan, Chem. Eng. Commun. **150**, 123 (1996).
[13] H. H. von Grunberg and R. Klein, J. Chem. Phys. **110**, 5421 (1999).
[14] T. Biben, P. Bladon, and D. Frenkel, J. Phys.: Condens. Matter **8**, 10 799 (1996).
[15] D. W. Siderius and D. S. Corti, following paper, Phys. Rev. E **71**, 036142 (2005).
[16] H. Reiss, H. M. Ellerby, and J. A. Manzanares, J. Phys. Chem. **100**, 5970 (1996).
[17] L. P. Chua, M.S. Thesis, Purdue University, West Lafayette, Indiana, 2002.
[18] E. Helfand, H. L. Frisch, and J. L. Lebowitz, J. Chem. Phys. **34**, 1037 (1961).
[19] M. J. Mandell and H. Reiss, J. Stat. Phys. **13**, 113 (1975).
[20] J. L. Lebowitz, E. Helfand, and E. Praestgaard, J. Chem. Phys. **43**, 774 (1965).
[21] R. C. Tolman, *Principles of Statistical Mechanics* (Oxford University Press, London, 1938).
[22] M. S. Wertheim, Phys. Rev. Lett. **10**, 321 (1963).
[23] M. D. Heying and D. S. Corti, J. Phys. Chem. B **108**, 19756 (2004).
[24] B. Götzelmann, R. Evans, and S. Dietrich, Phys. Rev. E **57**, 6785 (1998).
[25] B. Widom, J. Stat. Phys. **19**, 563 (1978).
[26] B. Widom, J. Phys. Chem. **86**, 869 (1982).
[27] N. F. Carnahan and K. E. Starling, J. Chem. Phys. **51**, 635 (1969).
[28] R. Bragado and G. Navascues, Phys. Rev. A **29**, 2134 (1984).
[29] R. Bragado and G. Navascues, J. Chem. Phys. **68**, 2971 (1979).
[30] J. E. Finn and P. A. Monson, Mol. Phys. **65**, 1345 (1988).
[31] J. E. Finn and P. A. Monson, Langmuir **5**, 639 (1989).
[32] D. Frenkel and B. Smit, *Understanding Molecular Simulation* (Academic, San Diego, 1996).
[33] S. Punnathanam and D. S. Corti, Ind. Eng. Chem. Res. **41**, 1113 (2002).
[34] B. J. Adler and T. E. Wainwright, J. Chem. Phys. **27**, 1208 (1957).
[35] W. W. Wood and J. D. Jacobson, J. Chem. Phys. **27**, 1207 (1957).
[36] W. G. Hoover and F. H. Ree, J. Chem. Phys. **48**, 3609 (1968).
[37] D. W. Siderius, M.S. thesis, Purdue University, West Lafayette, Indiana, 2004.